



Original Article

A study of thermomechanical behaviour and grain size evolution of AA7050 under hot forging conditions

Weishu Li ^a, Yaoqiong Liu ^{b, c}, Shuai Jiang ^a, Qinmeng Luan ^a, Yibo Li ^c, Bin Gu ^b, Zhusheng Shi ^{a, *}

^a Department of Mechanical Engineering, Imperial College London, London, SW7 2AZ, UK

^b AVIC the First Aircraft Institute, Xi'an, PR China

^c Central South University, Changsha, PR China

ARTICLE INFO

Article history:

Received 2 October 2018
Received in revised form
19 October 2018
Accepted 22 October 2018
Available online xxx

Keywords:

AA7050
Hot forging
Viscoplastic behaviour
Microstructural evolution
Dynamic recrystallisation
Grain size

ABSTRACT

A series of compression tests have been carried out using Gleeble (3800) thermomechanical simulator to investigate the viscoplastic behaviour of AA7050 as well as its microstructural characteristics under hot forging conditions. The thermomechanical tests were conducted at the temperatures of 350–450 °C with strain rates of 0.0005–0.5 s⁻¹, which covers the range of hot forging conditions for AA7050. Interrupted tests have also been carried out to track the microstructural evolution under various thermomechanical deformation conditions. Particular attention has been focused on the criteria of dynamic recrystallisation in AA7050 during the uniaxial compression at high temperatures, which could help to obtain regular homogeneous grain structures for hot forged components. It was found that AA7050 has a strong viscoplastic behaviour and flow stress is more than halved from 350 to 450 °C. A suitably low strain rate and high temperature are required for significant dynamic recrystallisation (0.05 s⁻¹ and 400 °C in current deformation level). The average grain size decreases with increasing strain and deformation temperature due to dynamic recrystallisation, but the relationship between average grain size and strain rate is not monotonic. Present findings provide a guideline for the selection of hot forging parameters so that quality components could be achieved with low forging force.

© 2018 The Authors. Production and hosting by Elsevier B.V. on behalf of KeAi Communications Co., Ltd. This is an open access article under the CC BY-NC-ND license (<http://creativecommons.org/licenses/by-nc-nd/4.0/>).

1. Introduction

7xxx series aluminium alloys with high strength-density ratio have been widely used in aeronautical and automobile industry, among which, the aluminium alloy 7050 (AA7050), a typical Al-Zn-Mg-Cu aluminium alloys, is particularly preferred because of its desirable physical and mechanical properties [1–3]. Good ductility during conventional forging under high temperature is another reason to explain the plentiful applications of high strength aluminium alloy in strength bearing critical airframe structural components of commercial airplanes [4,5]. However, the mechanical properties of large plate of high strength aluminium alloys are hugely influenced by complicated microstructural evolution during hot deformation [6], for example, average grain size has a strong influence on mechanical properties of aluminium alloys and coarse

grain structure will reduce the yield and strength limit of the material, thereby affecting the lifetime and performance of the components. The microstructural characteristics are mainly determined by deformation conditions [7,8], in other words, thermomechanical processing conditions play a very important role in the microstructural evolution of aluminium alloys during deformation. The control of microstructure during industrial manufacturing process is crucial for acquiring desirable properties of final product [9]. Therefore it is very important to investigate thermomechanical behaviour and microstructural evolution to improve understanding towards 7050 aluminium alloy. The softening mechanism of dynamic recrystallisation (DRX) that may occur during deformation of high stacking fault energy under high temperature is considered very important as it will generate uniform small size equiaxed grains and reduce the flow stress of the material, hence improving its forgeability [10].

For 7xxx series high strength aluminium alloys, most of the researches are focused on the heat treatment after forging and less

* Corresponding author.

E-mail address: zhusheng.shi@imperial.ac.uk (Z. Shi).

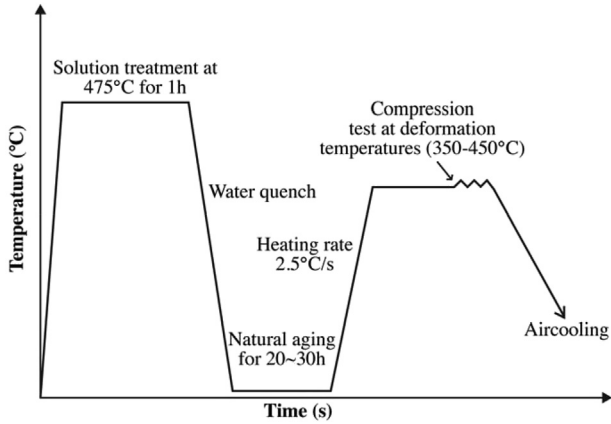


Fig. 1. Temperature profile for thermomechanical tests of AA7050.

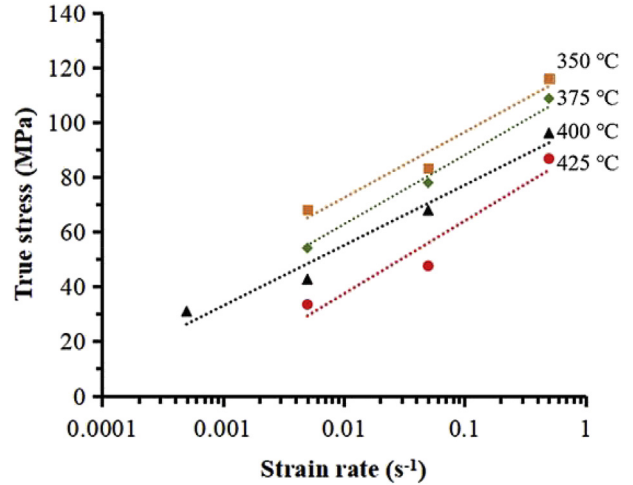
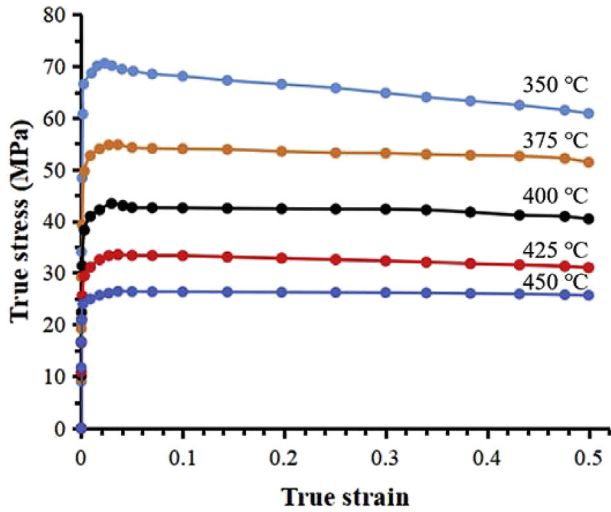
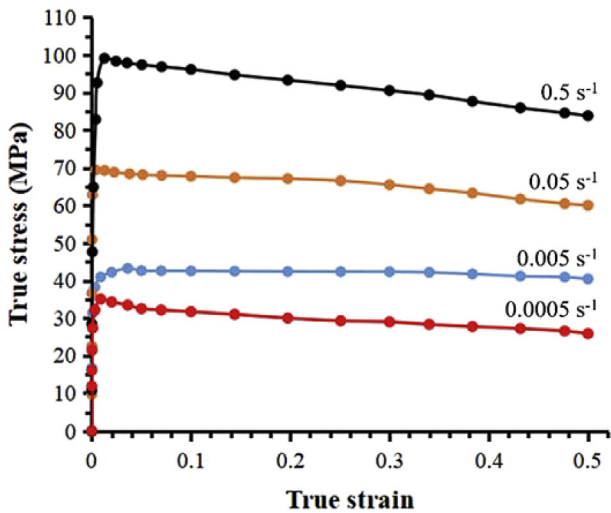


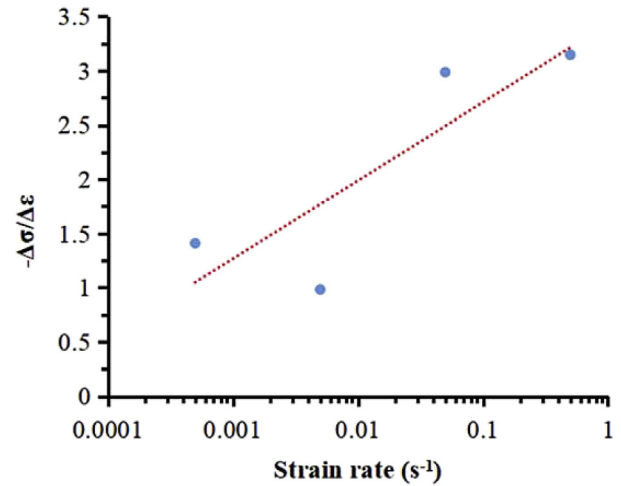
Fig. 3. Variation of flow stress with strain rates at true strain of 0.1 and different temperatures.



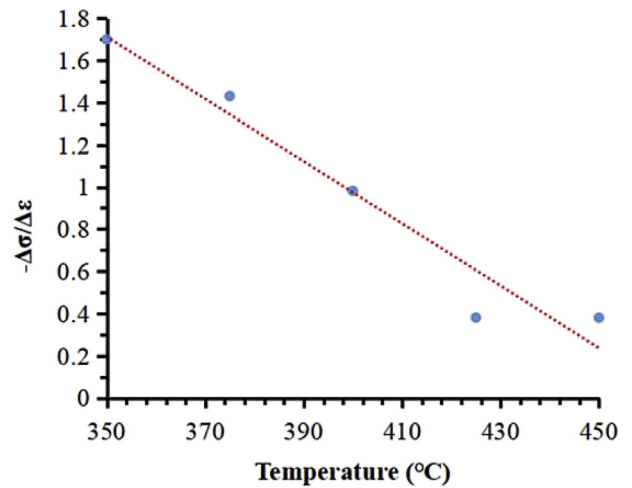
(a) At strain rate of 0.005 s^{-1} .



(b) At temperature of $400 \text{ }^\circ\text{C}$.



(a) At $400 \text{ }^\circ\text{C}$



(b) At $\dot{\epsilon} = 0.005 \text{ s}^{-1}$

Fig. 2. Flow stress of AA7050 at (a) different temperatures with strain rate of 0.005 s^{-1} and (b) different strain rates at $400 \text{ }^\circ\text{C}$.

Fig. 4. Softening of AA7050 at (a) different strain rates at $400 \text{ }^\circ\text{C}$ and (b) different temperatures with strain rate of 0.005 s^{-1} . The data were obtained at true strain of 0.3.

attention has been drawn to investigation involving microstructural evolution at elevated temperature [11–13]. A few reports about the misorientation transformation of aluminium alloys during hot deformation have been published, e.g. Hu et al. [6] investigated the microstructural evolution and hot deformation mechanism during hot forging for AA7050 Al alloy, Wang et al. [14] studied the effect of lattice diffusion and grain boundary diffusion under different conditions, and Deng et al. [7] studied the microstructure transformation of homogenised AA7050. Nevertheless, studies that link the grain size evolution to thermomechanical behaviour during deformation is still lacking.

The present work investigated temperature dependent flow stress behaviour of AA7050 under various deformation conditions, while interrupted compression tests have been performed for the characterisation of microstructural evolution of AA7050 during hot deformation. Optical microscopy has been employed to investigate microstructural evolution under different temperature and strain rates, particularly focusing on their influence on average grain size

variation. Electron backscatter diffraction (EBSD) technology has been used to examine the grain orientation map of the material and the potential dynamic recrystallisation during deformation, and the grain size distribution. The aim of this research is to acquire optimal parameters for hot forging by analysing the grain size evolution during deformation and provide guideline for industrial manufacturing process of AA7050.

2. Experimental procedure

The material used in the present work was a commercial AA7050 rolled thick plate with initial temper of T7451, whose main chemical composition is Al-6.2Zn-2.3Mg-2.3Cu-0.12Zr. Cylindrical specimens with 8 mm in diameter and 12 mm in height were machined from the plate for compression test. Thermomechanical tests were carried out using Gleeble 3800 thermomechanical simulation system with temperature range from 350 to 450 °C, and strain rates from 0.0005 to 0.5 s⁻¹. Interrupted compression tests

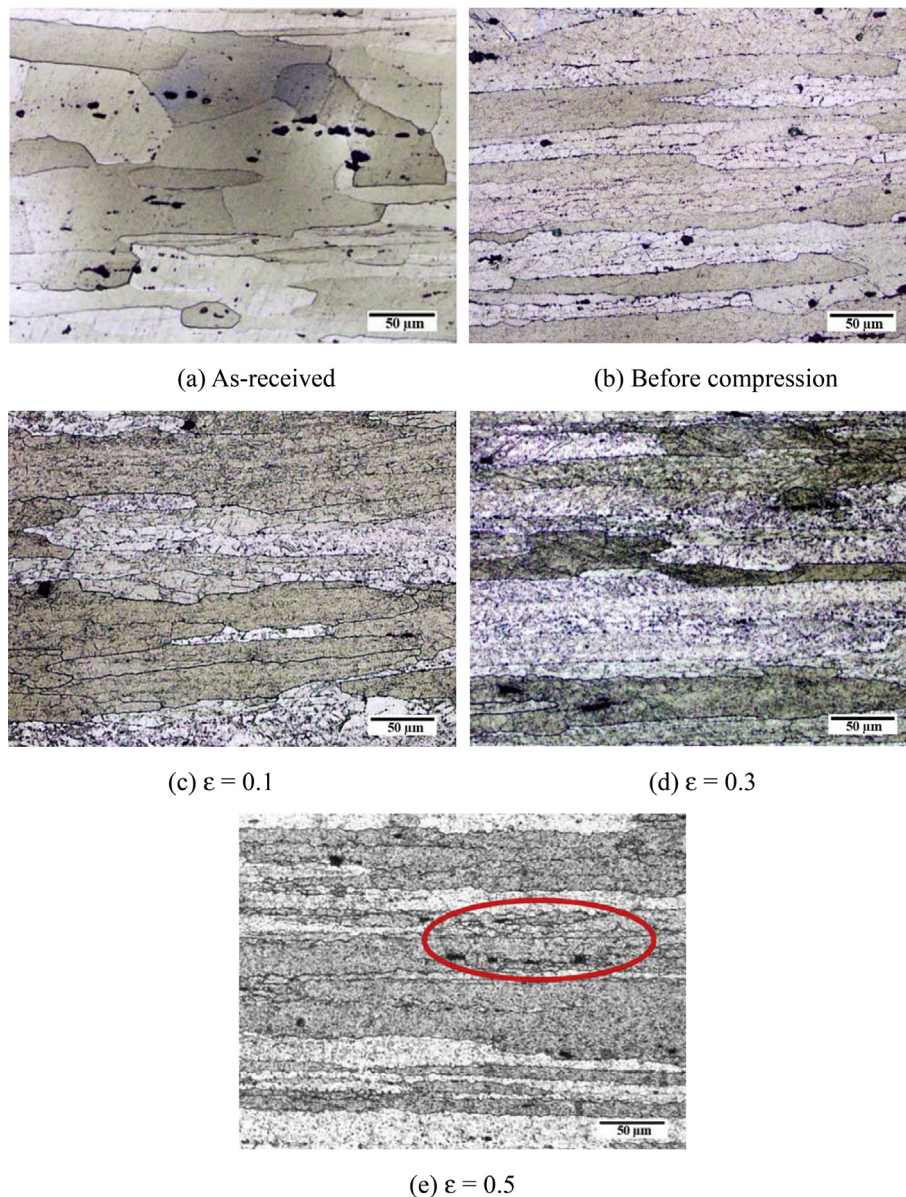


Fig. 5. Microstructural evolution at different stages of deformation at 400 °C and $\dot{\epsilon} = 0.05 \text{ s}^{-1}$: (a) As-received; (b) Before compression after heating and holding; and with compression strain of (c) 0.1; (d) 0.3; and (e) 0.5. The red circle indicates a recrystallised region. The compression is along the vertical direction of the micrographs, which is also the normal direction of the rolled plate.

were performed with strain of 0.1 and 0.3 to investigate the microstructural evolution of this material during hot deformation. The thermal history of the specimens is shown in Fig. 1. The specimens were solution heat treated at 475 °C for 1 h in an Instron furnace, then immersion quenched in water to room temperature, and naturally aged for 20–30 h. During compression tests, the specimens were heated up at a heating rate of 2.5 °C/s to target temperature in Gleeble machine and held for 3 min. The cylindrical specimens were then compressed from 12 to 7 mm in height (~42% reduction), followed by air cooling to room temperature.

The specimens were sectioned along axial direction, mounted in bakelite resin, grinded and polished to 1 μm . The prepared samples were then etched for 30 s using Keller's agent with composition of 1.5% HCl + 1% HF + 2.5% HNO₃ + 95% distilled water and cleaned with distilled water [15]. An Olympus BX53M optical microscope was used for microstructural examination. The specimens used for EBSD characterisation were grinded and polished with standard colloidal suspension for final polishing, a solution of 50% OPS + 50% water, using SAPHIR 520 metallographic grinder and polisher, and then electropolished using 10% perchloric acid and 90% ethanol solution with voltage of 17 V [16], which was determined by

optimised current, for 90 s at room temperature. The observation was carried out using FEI Quanta 650 equipped with Bruker eFlashHR EBSD system with accelerating voltage of 20 kV and step size of 2 μm [17,18]. The average grain size of the hot compression specimens was measured from the optical microscope images using Abrams Three-Circle procedure ASTM E112 [19]. The grain size was measured at three different locations for each specimen to minimise the effect of elongated grain structure. A deviation of 5 μm was found on grain size analysis and the result shown was the average of three measurements from different locations.

3. Results and discussion

3.1. Thermomechanical behaviour

The true stress–strain curve of AA7050 during hot compression under different temperatures and strain rates were obtained to show the thermomechanical behaviour of aluminium alloy 7050. According to previous researches, the mechanical properties of the material are closely related to the microstructure after compression [20–26], hence the microstructural evolution during hot deformation is analysed to obtain the optimum forging condition of

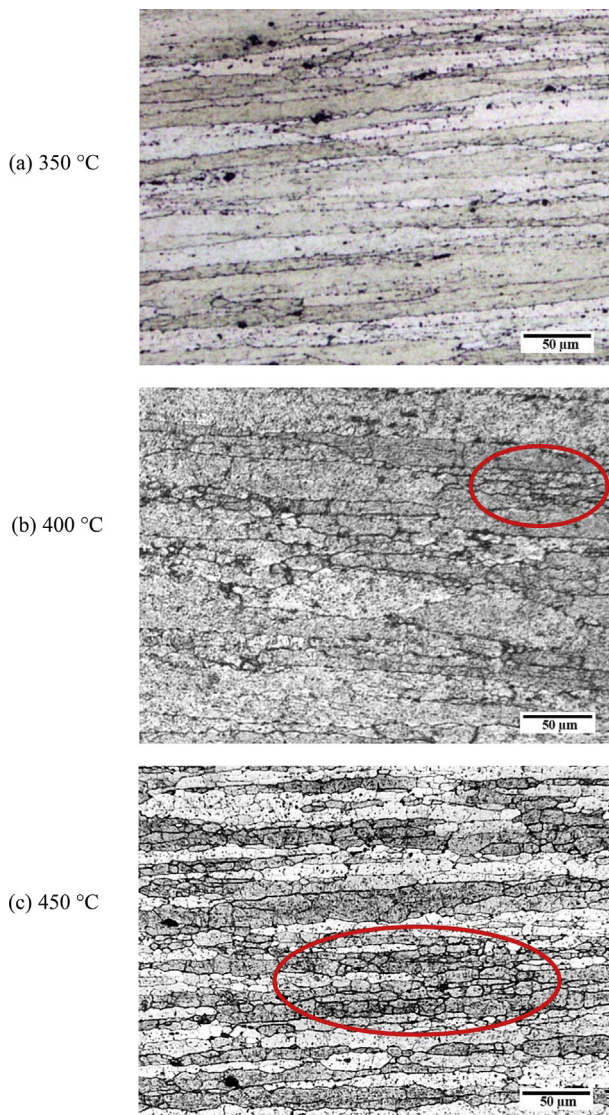


Fig. 6. Optical micrographs for materials deformed to $\epsilon = 0.5$ with $\dot{\epsilon} = 0.005 \text{ s}^{-1}$ at different temperatures: (a) 350 °C; (b) 400 °C; and (c) 450 °C.

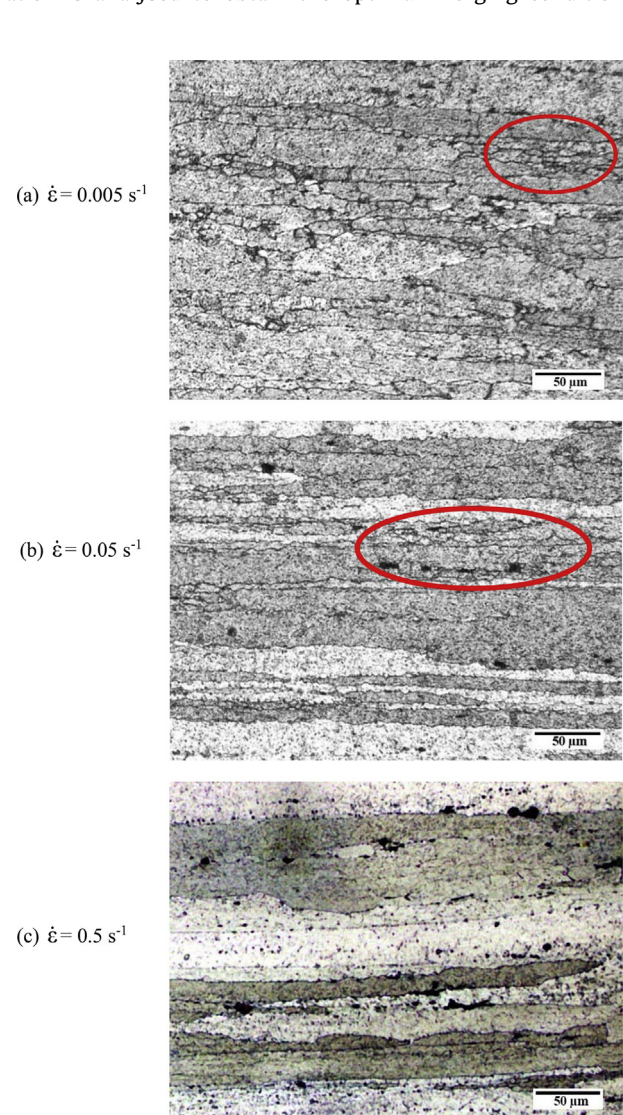


Fig. 7. Microstructural evolution for materials deformed to $\epsilon = 0.5$ at 400 °C with different strain rates: (a) 0.005 s^{-1} ; (b) 0.05 s^{-1} ; and (c) 0.5 s^{-1} .

this material. Fig. 2a shows the stress–strain curves of specimens deformed to the true strain of 0.5 with same strain rate of 0.005 s^{-1} at temperatures ranging from 350 to 450 °C, while Fig. 2b shows the stress–strain curves of specimens deformed at 400 °C with various strain rates $0.0005\text{--}0.5 \text{ s}^{-1}$. Generally, the true stress decreased with increasing deformation temperature and increased with increasing strain rate. Clear tendency can be observed that the true stress first rose rapidly to a plateau and then decreased to some extent, indicating that AA7050 has good uniform deformation ability. Strong viscoplastic behaviour is shown in Fig. 2b, as the strain rate decreased from 0.5 to 0.005 s^{-1} , a sharp decrease of stress occurs. The flow stress behaviour is therefore highly dependent on strain rate. Comparing with other conditions, lower true stress was observed at higher temperature range and lower strain rate range e.g. 400–450 °C and $0.0005\text{--}0.005 \text{ s}^{-1}$, suggesting a lower forging force during deformation at these conditions which is desirable for industry forging process.

The relationship between true stress and strain rate (logarithmic scale) at the true strain of 0.1 and different temperatures can be seen in Fig. 3. The trend lines are nearly straight and parallel to each other, and their angle from the x-axis was about 29°. The relationship between true stress and strain rate indicates the strong viscoplastic behaviour of AA7050 under different temperatures. With the decrease of strain rate from 0.5 to 0.005 s^{-1} , the stress decreased sharply by about 50% from 350 to 425 °C.

Fig. 4 shows the tangent slope variation from the stress–strain curves in Fig. 2 at the temperature of 400 °C and strain rate of 0.005 s^{-1} , deformed to the same true strain of 0.3. It can be seen that the slope of stress–strain curves generally increases with increasing strain rate and decreasing temperature. This phenomenon was considered as the effect of higher softening mechanism generated by possible dynamic recovery and dynamic recrystallisation influenced by deformation conditions, the material is in better plasticity with higher temperature and lower strain rate.

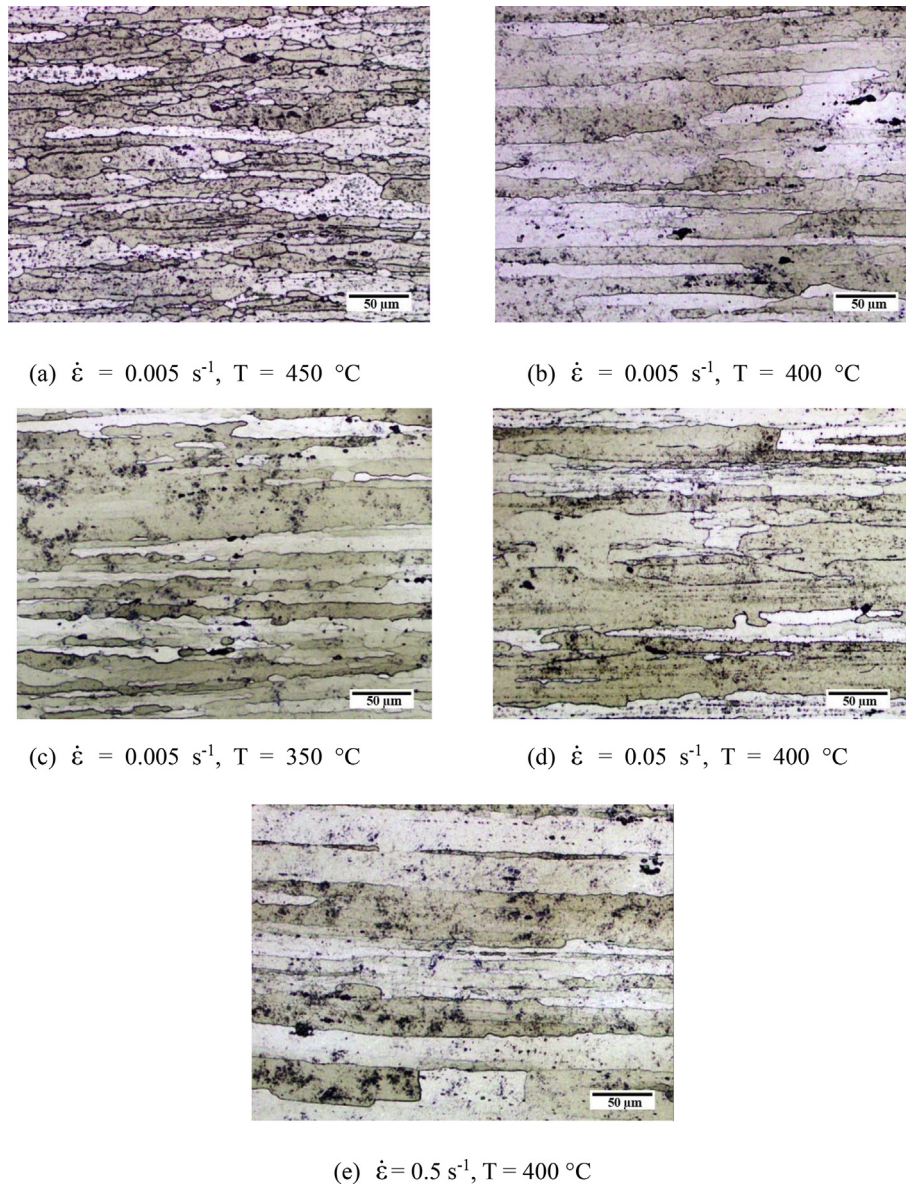


Fig. 8. Microstructural evolution after solution heat treatment of the material tested with: (a) (b) (c) different temperatures at $\dot{\epsilon} = 0.005 \text{ s}^{-1}$; (b) (d) (e) different strain rates at 400 °C.

3.2. Microstructural evolution and analysis

The microstructural evolution of AA7050 during compression test at 400 °C and 0.05 s⁻¹ is shown in Fig. 5 with a gradual transformation before and after deformation. It shows that the grains have a bandlike structure and coarse elongated grain were observed. Fig. 5a shows the microstructure of the as-received material with less obvious bandlike structure. Fig. 5b shows the microstructure after heating and holding in the Gleeble before Compression. The more elongated grain structure is believed to be introduced by the creep effect during heating and holding period before compression starts since a force of 0.5 kN was applied to ensure good conductivity for resistance heating. As the true strain increases, the deformation in grain structure becomes more and more severe, and the specimen with 0.5 true strain shows the most distinct bandlike grain structure. Small region of recrystallised grain structure could be observed at 0.5 true strain (see circled area in Fig. 5e), showing that dynamic recrystallisation (DRX) happened at this condition during deformation. No evident bimodal structure was detected in other specimens with lower strain at this temperature, implying that a critical strain is required for recrystallisation to occur at the above condition.

Fig. 6 shows the microstructural changes at strain rate of 0.005 s⁻¹ with different temperatures of 350, 400 and 450 °C. A clear gradual transformation from the squeezed elongated grain structure to bimodal structure could be seen with increasing deformation temperature. The grain structure was identified as recrystallisation (RX) region and elongated coarse grain region. The grain structure of the specimen deformed at 350 °C shown in Fig. 6a has coarse region only, while RX grain structure could be seen at condition of 400 °C (circled area in Fig. 6b) but in smaller region and lower extent. At 450 °C, a clear decomposition of elongated grains to smaller RX grains could be observed in Fig. 6c and the grain structure were fully recrystallised. Comparing with Fig. 6a and b where no clear sign of recrystallised grain structure was shown with lower deformation temperature, it can be seen that the increasing temperature was a factor that influenced the extent of dynamic recrystallisation. The microscopic results confirm that RX grain would appear under conditions from 400 to 450 °C and 0.005 s⁻¹ strain rate, which is good for industry processing as a lower force will be required for the forging operation at these conditions.

The microstructure at 400 °C with different strain rates of 0.005, 0.05 and 0.5 s⁻¹ are shown in Fig. 7. Small regions of RX grains are detected when the strain rate was at 0.005 and 0.05 s⁻¹. More recrystallised grain structures are found at 0.005 s⁻¹ than that of 0.05 s⁻¹, while no clear sign of RX region was detected under strain rate of 0.5 s⁻¹. It is also noticed that the recrystallised grains at 0.005 s⁻¹ seems more developed with larger size. The absence of RX grain structure at high strain rate was considered as the result of insufficient incubation time, since the occurrence of DRX needs enough time to release deformation energy. Therefore the strain rate is considered as another factor influencing the extent of DRX.

Solution heat treatment was carried out on selected specimens after hot compression test to analyse the effect of SHT on deformed microstructure of AA7050 and results are shown in Fig. 8. As shown in the figures, the grain size of all the specimens has generally grown larger but bandlike structure of grain still remains. Clearer grain boundary can be seen in Fig. 8 compared with the figures before solution heat treatment, and there is no clear sign of sub-grains. The small recrystallised grains at 0.05 and 0.005 s⁻¹ under 400 °C disappeared after SHT, suggesting that the RX grains grew and merged into larger grain structure during this process. Areas of recrystallised grain structure under 0.005 s⁻¹ and 450 °C can still be detected but with larger grain size. No static recrystallisation was detected in all deformed specimen after SHT.

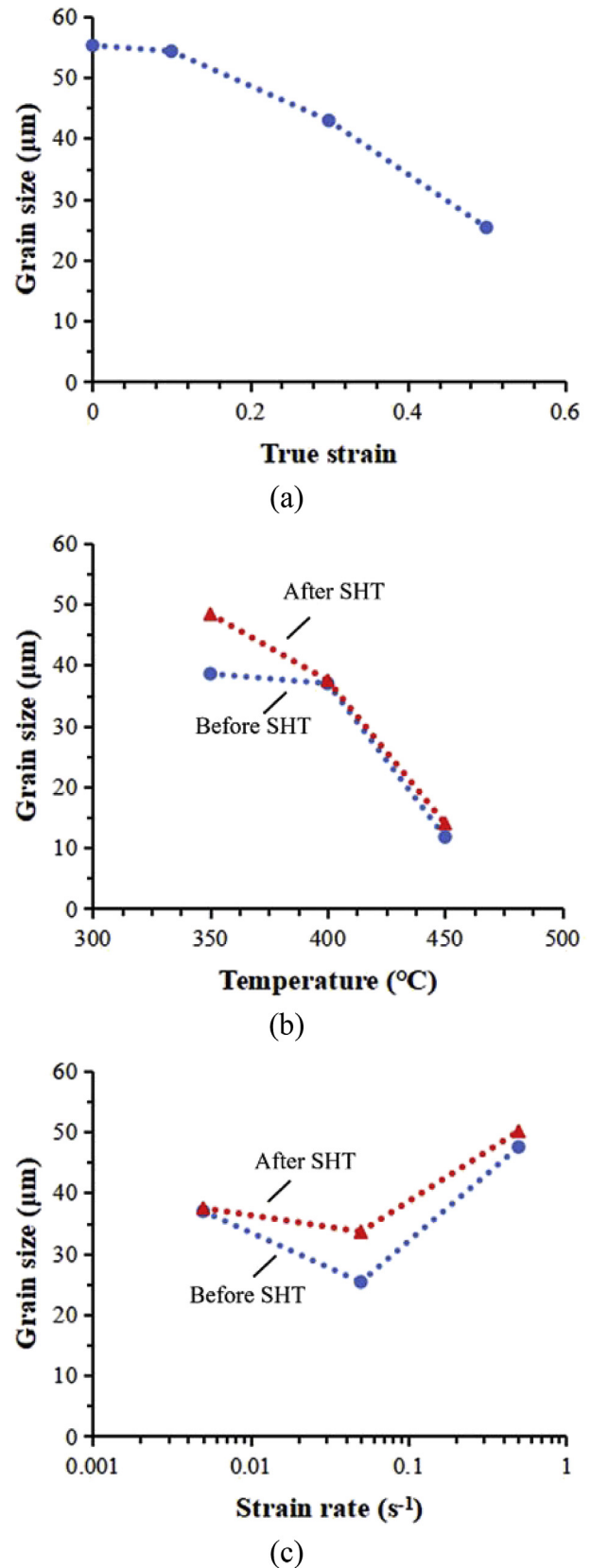


Fig. 9. Average grain size variation of the material (a) with true strains at 400 °C, $\dot{\epsilon} = 0.05 \text{ s}^{-1}$; (b) with temperatures, $\epsilon = 0.5$, $\dot{\epsilon} = 0.005 \text{ s}^{-1}$; (c) with strain rates, $\epsilon = 0.5$, 400 °C.

Fig. 9 shows the grain size variation with different true strains, strain rates and temperatures. The grain size of the original material was measured to be 55.25 μm , which is larger than the grain size of specimens deformed under all conditions. The relationship between grain size and true strain can be seen in Fig. 9a, in which the grain size gradually decreased with increasing true strain. As the strain increased, the specimen was deformed to a larger extent, and the elongated grains were further squeezed, which led to the decrease of average grain size. Another important factor that led to the decrease of grain size is the formation of recrystallised grains at larger strain, as shown in Fig. 5. Further analysis using EBSD need be performed to analyse the grain size transformation during deformation.

Fig. 9b shows the effect of deformation temperature on average grain size. The grain size was slightly decreased between temperature of 350 $^{\circ}\text{C}$ and 400 $^{\circ}\text{C}$, and rapidly decreased between 400 $^{\circ}\text{C}$ and 450 $^{\circ}\text{C}$. This variation of grain size was due to the occurrence of recrystallisation between deformation temperatures of 400 and 450 $^{\circ}\text{C}$. When the deformation temperature was low (350–400 $^{\circ}\text{C}$), the average grain size variation was not significant and the dynamic recovery was the driving softening mechanism. When the deformation temperature was higher (400–450 $^{\circ}\text{C}$), dynamic recrystallisation occurred during deformation, the subgrains merged and grew to replace original grains during this process [27], causing grain refinement and therefore rapidly decreasing the average grain size. Compared with the microscopic results at 350–450 $^{\circ}\text{C}$ under strain rate of 0.005 s^{-1} shown in Fig. 6, the small average grain size at 400 and 450 $^{\circ}\text{C}$ are consistent with the occurrence of recrystallised grain structure at these temperatures.

The effect of strain rate on average grain size is not monotonic, as shown in Fig. 9c. With increasing strain rate, the average grain size decreased between strain rates of 0.005 and 0.05 s^{-1} , and then

increased between strain rates of 0.05 and 0.5 s^{-1} . According to the optical microstructure characterisation result, dynamic recrystallisation took place at temperature of 400 $^{\circ}\text{C}$ and strain rate below 0.05 s^{-1} (see Fig. 7). With the decreasing strain rate from 0.5 to 0.05 s^{-1} , recrystallisation occurred, resulting in lower average grain size. The increase of average grain size between strain rate of 0.05 and 0.005 s^{-1} is possibly due to the growth of the recrystallised grains, evidenced by comparing Fig. 7a and b.

Fig. 10 shows the IPFX colouring maps for specimens deformed at strain rates of 0.05 and 0.5 s^{-1} at 400 $^{\circ}\text{C}$ from EBSD results. Fig. 10a and b demonstrate the effect of deformation (strain level) on recrystallisation. Little sign of recrystallised grain structure could be seen in Fig. 10a when the strain was 0.3 under 0.05 s^{-1} . As deformation continues to the true strain of 0.5, the grain structure were highly deformed and small regions of recrystallised grain structure could be observed (Fig. 10b). For the material deformed to 0.5 strain at 0.5 s^{-1} in Fig. 10c, no RX structure was observed, which indicates the important effect of strain rate on recrystallisation. The results in Fig. 10 confirms that a certain degree of deformation and a suitably low strain rate are required for AA7050 to form recrystallised structure at 400 $^{\circ}\text{C}$.

The grain size distributions for these specimens have been measured and are shown in Fig. 11. Comparison of Fig. 11a and b shows that as deformation continued and the strain increased from 0.3 to 0.5, the fraction of large size grains decreased while that of the small size grain increased markedly, indicating that the RX structure increased sharply during deformation. With the breaking of large grains and the generation of RX grains, the average grain size was decreasing during this period, consistent with average grain size variation shown in Fig. 9a. For the specimen with 0.5 s^{-1} and 0.5 strain, results show that very few small recrystallised grains are present and there is a large grain area up to $7 \times 10^4 \mu\text{m}^2$,

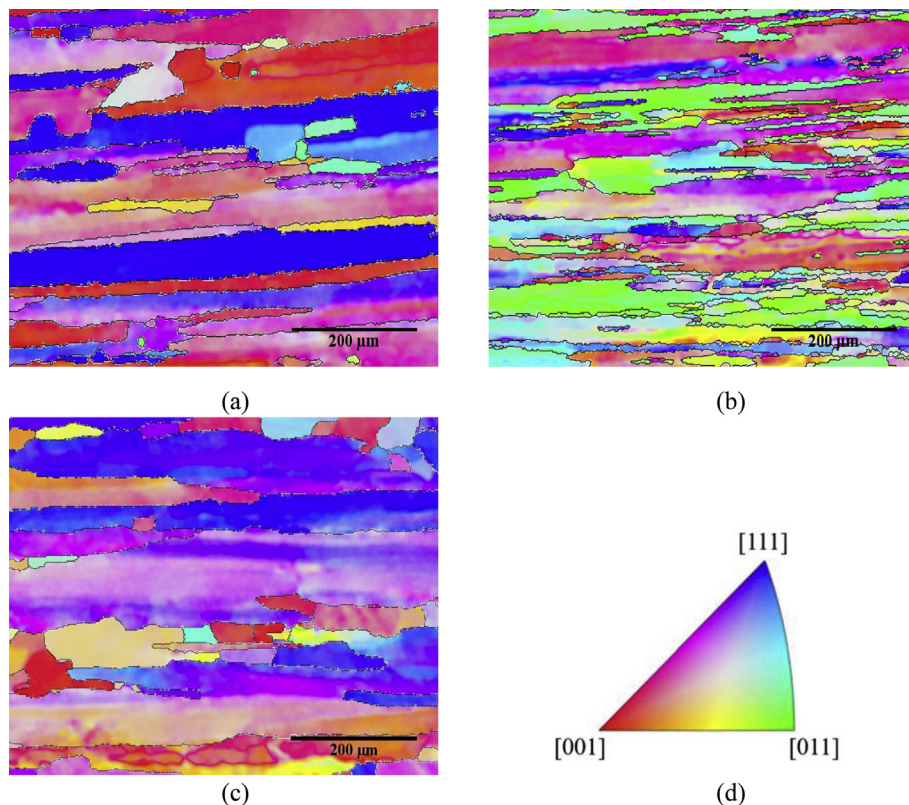


Fig. 10. EBSD maps (IPFX colouring) of specimens deformed at 400 $^{\circ}\text{C}$ with: (a) 0.3 strain, 0.05 s^{-1} ; (b) 0.5 strain, 0.05 s^{-1} ; (c) 0.5 strain, 0.5 s^{-1} ; (d) Crystallographic orientation colour key.

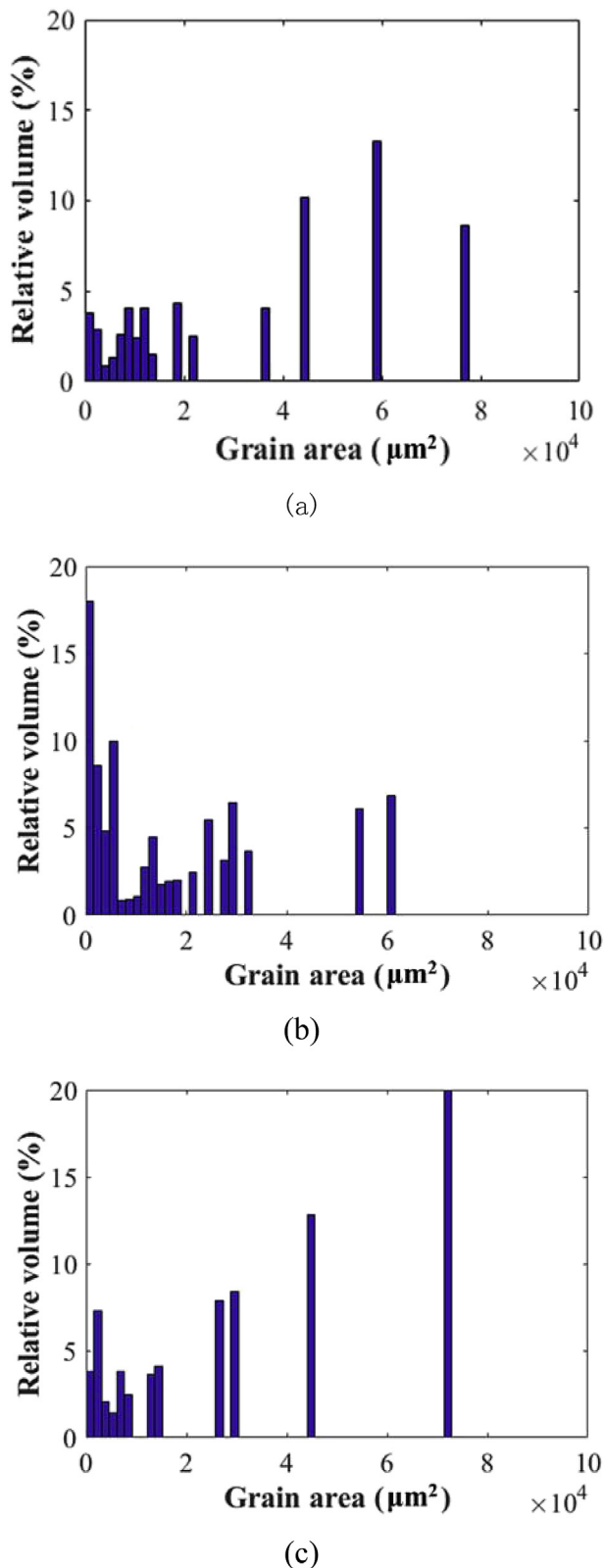


Fig. 11. Grain size distribution (μm^2) of specimens deformed at 400 °C: (a) 0.05 s^{-1} , 0.3 strain; (b) 0.05 s^{-1} , 0.5 strain; (c) 0.5 s^{-1} , 0.5 strain.

suggesting no obvious recrystallised grain structure at this condition. These results are consistent with optical microscopic observation, again confirming that a strain rate less than 0.05 s^{-1} is required for significant dynamic recrystallisation of AA7050 at 400 °C in the current deformation range.

4. Conclusions

Thermomechanical behaviour and microstructural evolution of AA7050 have been investigated under hot forging conditions, employing Gleeble thermomechanical simulator, optical microscopy and SEM-EBSD. The following conclusions can be drawn:

- (1) Clear sign of recrystallization has been detected for AA7050 under deformation conditions of 0.05 s^{-1} at 400 °C. Once the deformation temperature is increased to 450 °C and the strain rate is reduced to 0.005 s^{-1} , fully recrystallised structure can be obtained. The results suggest that the material should be hot forged at a temperature above 400 °C and a strain rate below 0.05 s^{-1} to obtain fully recrystallised structures.
- (2) Grain size variation of specimens under different deformation conditions has been compared. The average grain size decreases with increasing deformation temperature and true strain (deformation level); while the relationship between strain rate and average grain size is not monotonic.
- (3) Strong viscoplastic behaviour of the material has been observed at the hot forging conditions. If the strain rate drops from 0.5 to 0.005 s^{-1} , the flow stress could be reduced by 50% at 400 °C. When the temperature is increased from 350 to 450 °C, the flow stress is more than halved. It is recommended that the forging of the alloy should be carried out between 400 and 450 °C with strain rates of $0.0005\text{--}0.005 \text{ s}^{-1}$. At these conditions, dynamic recrystallisation could occur, which generates more uniform grain structures, and forging force could be halved, which results in less capacity presses required for forging large components.

Acknowledgements

The strong support from the Aviation Industry Corporation of China (AVIC) the First Aircraft Institute (FAI) for this funded research is much appreciated. The research was performed at the AVIC Centre for Structural Design and Manufacture at Imperial College London. The authors are also grateful for the support from China Scholarship Council.

References

- [1] A. Deschamps, Y. Bréchet, Influence of quench and heating rates on the ageing response of an Al–Zn–Mg–(Zr) alloy, *Mater. Sci. Eng. A* 251 (1–2) (1998) 200–207.
- [2] M. Tajally, E. Emadoddin, Mechanical and anisotropic behaviors of 7075 aluminum alloy sheets, *Mater. Des.* 32 (3) (2011) 1594–1599.
- [3] A. Rao, V. Vasu, M. Govindaraju, K. Srinadh, Stress corrosion cracking behaviour of 7xxx aluminum alloys: a literature review, *Trans. Nonferrous Metals Soc. China* 26 (6) (2016) 1447–1471.
- [4] Yashpal, C.S. Jawalkar, S. Kant, A review on use of aluminium alloys in Aircraft components, *i-manager's J. Mater. Sci.* 3 (3) (2015) 33–38.
- [5] K. Zheng, D. Politis, L. Wang, J. Lin, A review on forming techniques for manufacturing lightweight complex-shaped aluminium panel components, *Int. J. Lightweight Mater. Manuf.* 1 (2) (2018) 55–80.
- [6] H. Hu, L. Zhen, L. Yang, W. Shao, B. Zhang, Deformation behavior and microstructure evolution of 7050 aluminum alloy during high temperature deformation, *Mater. Sci. Eng. A* 488 (1–2) (2008) 64–71.
- [7] Y. Deng, Z. Yin, J. Huang, Hot deformation behavior and microstructural evolution of homogenized 7050 aluminum alloy during compression at elevated temperature, *Mater. Sci. Eng. A* 528 (3) (2011) 1780–1786.

- [8] N. Nayan, N. Gurao, S. Narayana Murty, A. Jha, B. Pant, S. Sharma, K. George, Microstructure and micro-texture evolution during large strain deformation of an aluminium–copper–lithium alloy AA 2195, *Mater. Des.* 65 (2015) 862–868.
- [9] L. Yan, J. Shen, J. Li, Z. Li, Z. Tang, Dynamic recrystallization of 7055 aluminum alloy during hot deformation, *Mater. Sci. Forum* 650 (2010) 295–301.
- [10] J. Li, J. Shen, X. Yan, B. Mao, L. Yan, Microstructure evolution of 7050 aluminum alloy during hot deformation, *Trans. Nonferrous Metals Soc. China* 20 (2) (2010) 189–194.
- [11] P. Rometsch, Y. Zhang, S. Knight, Heat treatment of 7xxx series aluminium alloys—some recent developments, *Trans. Nonferrous Metals Soc. China* 24 (7) (2014) 2003–2017.
- [12] A. Isadare, B. Aremo, M. Adeoye, O. Olawale, M. Shittu, Effect of heat treatment on some mechanical properties of 7075 aluminium alloy, *Mater. Res.* 16 (1) (2012) 190–194.
- [13] X. Wang, Q. Pan, L. Liu, S. Xiong, W. Wang, J. Lai, Y. Sun, Z. Huang, Characterization of hot extrusion and heat treatment on mechanical properties in a spray formed ultra-high strength Al-Zn-Mg-Cu alloy, *Mater. Char.* 144 (2018) 131–140.
- [14] S. Wang, J. Luo, L. Hou, J. Zhang, L. Zhuang, Physically based constitutive analysis and microstructural evolution of AA7050 aluminum alloy during hot compression, *Mater. Des.* 107 (2016) 277–289.
- [15] Metallographic.com, Metallographic etchants for aluminum alloys, 2006 [online] Available at: <http://www.metallographic.com/Etchants/Aluminum%20etchants.htm>. (Accessed 30 August 2018).
- [16] Y. Xu, L. Zhan, M. Huang, C. Liu, X. Wang, Anisotropy in creep-ageing behavior of textured Al-Cu-Mg alloy, *Int. J. Lightweight Mater. Manuf.* 1 (1) (2018) 40–46.
- [17] T. Sun, A. Reynolds, M. Roy, P. Withers, P. Prangnell, The effect of shoulder coupling on the residual stress and hardness distribution in AA7050 friction stir butt welds, *Mater. Sci. Eng. A* 735 (2018) 218–227.
- [18] S. Lim, I. Eun, S. Nam, Control of equilibrium phases (M,T,S) in the modified aluminum alloy 7175 for thick forging applications, *Mater. Trans.* 44 (1) (2003) 181–187.
- [19] Standard Test Methods for Determining Average Grain Size Using Semi-automatic and Automatic Image Analysis, ASTM International, West Conshohocken, PA, 2004.
- [20] M. Wang, W. Wang, J. Zhou, X. Dong, Y. Jia, Strain effects on microstructure behavior of 7050-H112 aluminum alloy during hot compression, *J. Mater. Sci.* 47 (7) (2011) 3131–3139.
- [21] H. Nagaum, T. Umeda, Study of the crack sensitivity of 6xxx and 7xxx aluminum alloys, *Mater. Sci. Forum* 426–432 (2003) 465–470.
- [22] Y. Liu, Q. Guo, C. Li, Y. Mei, X. Zhou, Y. Huang, H. Li, Recent progress on evolution of precipitates in inconel 718 superalloy, *Acta Metall.* 52 (10) (2016) 1259–1266.
- [23] N. Jin, H. Zhang, Y. Han, W. Wu, J. Chen, Hot deformation behavior of 7150 aluminum alloy during compression at elevated temperature, *Mater. Char.* 60 (6) (2009) 530–536.
- [24] G. Quan, K. Liu, J. Zhou, B. Chen, Dynamic softening behaviors of 7075 aluminum alloy, *Trans. Nonferrous Metals Soc. China* 19 (2009) s537–s541.
- [25] A. Scari, B. Pockszevnicki, J. Landre Junior, P. Magalhaes Junior, Stress-strain compression of AA6082-T6 aluminum alloy at room temperature, *J. Struct.* 2014 (2014) 1–7.
- [26] R. Pan, Z. Shi, C. Davies, C. Li, M. Kaye, J. Lin, An integrated model to predict residual stress reduction by multiple cold forging operations in extra-large AA7050 T-section panels, *Proc. IMechE Part B J. Eng. Manuf.* 232 (8) (2016) 1319–1330.
- [27] H. Raimbourg, T. Kogure, T. Toyoshima, Crystal bending, subgrain boundary development, and recrystallization in orthopyroxene during granulite-facies deformation, *Contrib. Mineral. Petrol.* 162 (5) (2011) 1093–1111.